$$d_i = [\pi\lambda\Delta/2]^{1/2} \qquad (4.3.8.21)$$

is known as the information resolution limit (see Subsection 4.3.8.6) and depends on electronic instabilities and the thermal-energy spread of electrons leaving the filament. The reduction in the contribution of particular diffracted beams to the image due to limited spatial coherence is minimized over those extended regions for which $\nabla\chi(\mathbf{u})$ is small, called passbands, which occur when

$$\Delta f_n = [C_s\lambda(8n+3)/2]^{1/2}. \qquad (4.3.8.22)$$

The Scherzer focus Δf_s corresponds to $n = 0$. These passbands become narrower and move to higher $\mathbf{u}$ values with increasing n, but are subject also to chromatic damping effects. The passbands occur between spatial frequencies U_1 and U_2, where

$$U_{1,2} = C_s^{-1/4}\lambda^{-3/4}\{[(8n+2)/2]^{1/2} \pm 1\}^{1/2}. \qquad (4.3.8.23)$$

Their use for extracting information beyond the point resolution of an electron microscope is further discussed in Subsection 4.3.8.6.

Fig. 4.3.8.5 shows transfer functions for a modern instrument for $n = 0$ and 1. Equations (4.3.8.14) and (4.3.8.17) provide a simple, useful, and popular approach to the interpretation of HREM images and valuable insights into resolution-limiting factors. However, it must be emphasized that these results apply only (amongst other conditions) for $\Phi_0 \gg \Phi_{\mathbf{g}}$ (in crystals) and therefore do not apply to the usual case of strong multiple electron scattering. Equation (4.3.8.13*b*) does not make this approximation. In real space, for crystals, the alignment of columns of atoms in the beam direction rapidly leads to phase changes in the electron wavefunction that exceed $\pi/2$, leading to the failure of equation (4.3.8.14). Accurate quantitative comparisons of experimental and simulated HREM images must be based on equation (4.3.8.13*a*), or possibly (4.3.8.13*b*), with $\psi(\mathbf{u}', \Delta f, \mathbf{r})$ obtained from many-beam dynamical calculations of the type described in Subsection 4.3.8.5.

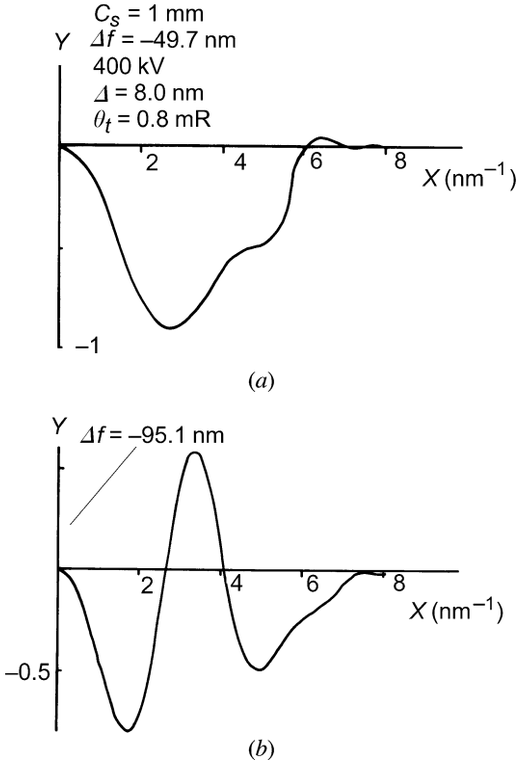

Fig. 4.3.8.5. (*a*) The transfer function for a 400 kV electron microscope with a point resolution of 1.7 Å at the Scherzer focus; the curve is based on equation (4.3.8.17). In (*b*) is shown a transfer function for similar conditions at the first 'passband' focus [$n = 1$ in equation (4.3.8.22)].

For the structure imaging of specific types of defects and materials, the following references are relevant. (i) For line defects viewed parallel to the line, d'Anterroches & Bourret (1984); viewed normal to the line, Alexander, Spence, Shindo, Gottschalk & Long (1986). (ii) For problems of variable lattice spacing (*e.g.* spinodal decomposition), Cockayne & Gronsky (1981). (iii) For point defects and their ordering, in tunnel structures, Yagi & Cowley (1978); in semiconductors, Zakharov, Pasemann & Rozhanski (1982); in metals, Fields & Cowley (1978). (iv) For interfaces, see the proceedings reported in *Ultramicroscopy* (1992), Vol. 40, No. 3. (v) For metals, Lovey, Coene, Van Dyck, Van Tendeloo, Van Landuyt & Amelinckx (1984). (vi) For organic crystals, Kobayashi, Fujiyoshi & Uyeda (1982). (vii) For a general review of applications in solid-state chemistry, see the collection of papers reported in *Ultramicroscopy* (1985), Vol. 18, Nos. 1–4. (viii) Radiation-damage effects are observed at atomic resolution by Horiuchi (1982).

4.3.8.4. *Parameters affecting HREM images*

The *instrumental parameters* that affect HREM images include accelerating voltage, astigmatism, optic-axis alignment, focus setting Δf, spherical-aberration constant C_s, beam divergence θ_c, and chromatic aberration constant C_c. Crystal parameters influencing HREM images include thickness, absorption, ionicity, and the alignment of the crystal zone axis with the beam, in addition to the structure factors and atom positions of the sample. The accurate measurement of electron wavelength or accelerating voltage has been discussed by many workers, including Uyeda, Hoier and others [see Fitzgerald & Johnson (1984) for references]. The measurement of Kikuchi-line spacings from crystals of known structure appears to be the most accurate and convenient method for HREM work, and allows an overall accuracy of better than 0.2% in accelerating voltage. Fluctuations in accelerating voltage contribute to the chromatic damping term Δ in equation (4.3.8.19) through the variance $\sigma^2(V_0)$. With the trend toward the use of higher accelerating voltages for HREM work, this term has become especially significant for the consideration of the information resolution limit [equation (4.3.8.21)].

Techniques for the accurate measurement of astigmatism and chromatic aberration are described by Spence (1988). The displacement of images of small crystals with beam tilt may be used to measure C_s; alternatively, the curvature of higher-order Laue-zone lines in CBED patterns has been used. The method of Budinger & Glaeser (1976) uses a similar dark-field image-displacement method to provide values for both Δf and C_s, and appears to be the most convenient and accurate for HREM work. The analysis of optical diffractograms initiated by Thon and co-workers from HREM images of thin amorphous films provides an invaluable diagnostic aid for HREM work; however, the determination of C_s by this method is prone to large errors, especially at small defocus. Diffractograms provide a rapid method for the determination of focus setting (see Krivanek, 1976) and in addition provide a sensitive indicator of specimen movement, astigmatism, and the damping-envelope constants Δ and Θ_c.

Misalignment of the electron beam, optic axis, and crystal axis in bright-field HREM work becomes increasingly important with increasing resolution and specimen thickness. The first-order effects of optical misalignment are an artifactual translation of spatial frequencies in the direction of misalignment by an amount proportional to the misalignment and to the square of spatial frequency. The corresponding phase shift is not observable in diffractograms. The effects of astigmatism on transfer functions for inclined illumination are discussed in Saxton (1978).

The effects of misalignment of the beam with respect to the optic axis are discussed in detail by Smith, Saxton, O'Keefe, Wood & Stobbs (1983), where it is found that all symmetry elements (except a mirror plane along the tilt direction) may be destroyed by misalignment. The maximum allowable misalignment for a given resolution δ in a specimen of thickness t is proportional to

$$\alpha = \delta/8t. \qquad (4.3.8.24)$$

Misalignment of a crystalline specimen with respect to the beam may be distinguished from misalignment of the optic axis with respect to the beam by the fact that, in very thin crystals, the former does not destroy centres of symmetry in the image.

The use of known defect point-group symmetry (for example in stacking faults) to identify a point in a HREM image with a point in the structure and so to resolve the black or white atomic contrast ambiguity has been described (Olsen & Spence, 1981). Structures containing screw or glide elements normal to the beam are particularly sensitive to misalignment, and errors as small as 0.2 mrad may substantially alter the image appearance.

A rapid comparison of images of amorphous material with the beam electronically tilted into several directions appears to be the best current method of aligning the beam with the optic axis, while switching to convergent-beam mode appears to be the most effective method of aligning the beam with the crystal axis. However, there is evidence that the angle of incidence of the incident beam is altered by this switching procedure.

The effects of misalignment and choice of beam divergence Θ_c on HREM images of crystals containing dynamically forbidden reflections are reviewed by Nagakura, Nakamura & Suzuki (1982) and Smith, Bursill & Wood (1985). Here the dramatic example of rutile in the [001] orientation is used to demonstrate how a misalignment of less than 0.2 mrad of the electron beam with respect to the crystal axis can bring up a coarse set of fringes (4.6 Å), which produce an image of incorrect symmetry, since these correspond to structure factors that are forbidden both dynamically and kinematically.

Crystal thickness is most accurately determined from images of planar faults in known orientations, or from crystal morphology for small particles. It must otherwise be treated as a refinement parameter. Since small crystals (such as MgO smoke particles, which form as perfect cubes) provide such an independent method of thickness determination, they provide the most convincing test of dynamical imaging theory. *The ability to match the contrast reversals and other detailed changes in HREM images as a function of either thickness or focus (or both) where these parameters have been measured by an independent method gives the greatest confidence in image interpretation*. This approach, which has been applied in rather few cases [see, for example, O'Keefe, Spence, Hutchinson & Waddington (1985)] is strongly recommended. The tendency for n-beam dynamical HREM images to repeat with increasing thickness in cases where the wavefunction is dominated by just two Bloch waves has been analysed by several workers (Kambe, 1982).

Since electron scattering factors are proportional to the difference between atomic number and X-ray scattering factors, and inversely proportional to the square of the scattering angle (see Section 4.3.1), it has been known for many years that the low-order reflections that contribute to HREM images are extremely sensitive to the distribution of bonding electrons and so to the degree of ionicity of the species imaged. This observation has formed the basis of several charge-density-map determinations by convergent-beam electron diffraction [see, for example, Zuo, Spence & O'Keefe (1988)]. Studies of ionicity effects on HREM imaging can be found in Anstis, Lynch, Moodie & O'Keefe (1973) and Fujiyoshi, Ishizuka, Tsuji, Kobayashi & Uyeda (1983).

The depletion of the elastic portion of the dynamical electron wavefunction by inelastic crystal excitations (chiefly phonons, single-electron excitations, and plasmons) may have dramatic effects on the HREM images of thicker crystals (Pirouz, 1974). For image formation by the elastic component, these effects may be described through the use of a complex 'optical' potential and the appropriate Debye–Waller factor (see Section 2.5.1). However, existing calculations for the absorption coefficients derived from the imaginary part of this potential are frequently not applicable to lattice images because of the large objective apertures used in HREM work. It has been suggested that HREM images formed from electrons that suffer small energy losses (and so remain 'in focus') but large-angle scattering events (within the objective aperture) due to phonon excitation may contribute high-resolution detail to images (Cowley, 1988). For measurements of the imaginary part of the optical potential by electron diffraction, the reader is referred to the work of Voss, Lehmpfuhl & Smith (1980), and references therein. All evidence suggests, however, that for the crystal thicknesses generally used for HREM work ($t < 200$ Å) the effects of 'absorption' are small.

In summary, the general approach to the matching of computed and experimental HREM images proceeds as follows (Wilson, Spargo & Smith, 1982). (i) Values of Δ, Θ_c, and C_s are determined by careful measurements under well defined conditions (electron-gun bias setting, illumination aperture size, specimen height as measured by focusing-lens currents, electron-source size, *etc*). These parameters are then taken as constants for all subsequent work under these instrumental conditions (assuming also continuous monitoring of electronic instabilities). (ii) For a particular structure refinement, the parameters of thickness and focus are then varied, together with the choice of atomic model, in dynamical computer simulations until agreement is obtained. Every effort should be made to match images as a function of thickness and focus. (iii) If agreement cannot be obtained, the effects of small misalignments must be investigated (Smith *et al.*, 1985). Crystals most sensitive to these include those containing reflections that are absent due to the presence of screw or glide elements normal to the beam.

4.3.8.5. *Computing methods*

The general formulations for the dynamical theory of electron diffraction in crystals have been described in Section 5.2 of *IT* B (1992). In Section 4.3.6, the computing methods used for calculating diffraction-beam amplitudes have been outlined.

Given the diffracted-beam amplitudes, $\Psi_{\mathbf{g}}$, the image is calculated by use of equations (4.3.8.2), including, when appropriate, the modifications of (4.3.8.13*b*).

The numerical methods that can be employed in relation to crystal-structure imaging make use of algorithms based on (i) matrix diagonalization, (ii) fast Fourier transforms, (iii) real-space convolution (Van Dyck, 1980), (iv) Runge-Kutta (or similar) methods, or (v) power-series evaluation. Two other solutions, the Cowley–Moodie polynomial solution and the

references